Research article

Therapeutic mechanisms of modified Jiawei Juanbi decoction in early knee osteoarthritis: A multimodal analysis

Kun Gao [a],[*],[1], Zhenyu Huang [b],[1], Weiji Yu [a], Yihong Wu [a], Weidong Liu [a], Shufen Sun [a], Yong Zhang [a], Dayu Chen [a]

[a] *Shenzhen Traditional Chinese Medicine Hospital, Shenzhen, 518033, China*
[b] *The Fourth Clinical Medical College of Guangzhou University of Chinese Medicine, Guangzhou, 510006, China*

ARTICLE INFO

ABSTRACT

Modified Jiawei Juanbi decoction (MJD) is used for the treatment of early-stage knee osteoarthritis (KOA). Here, modified Jiawei Juanbi decoction (MJD) was employed for the treatment of early-stage knee osteoarthritis (KOA) and its mechanisms were assessed via metabonomics and network pharmacology. A total of 24 male Sprague-Dawley rats were randomly allocated into a normal control group, a model group, and an MJD group (n = 8 rats per group). Each rat group was further equally divided into two subgroups for investigation for either 14 or 28 days. A rat model of early-stage KOA was constructed and rats were treated with MJD. Effects were evaluated based on changes in knee circumference, mechanical withdrawal threshold (MWT) and thermal withdrawal latency (TWL). We also analyzed histopathological changes in articular cartilage. High-resolution mass spectrometry was used to analyze the chemical profile of MJD, identifying 228 components. Using an LC-Q-TOF-MS metabonomics approach, 33 differential metabolites were identified. The relevant pathways significantly associated with MJD include arginine and proline metabolism, vitamin B6 metabolism, as well as the biosynthesis of phenylalanine, tyrosine and tryptophan. The system pharmacology paradigm revealed that MJD contains 1027 components and associates with 1637 genes, of which 862 disease genes are related to osteoarthritis. The construction of the MJD composition-target-KOA network revealed a total of 140 intersection genes. A total of 39 hub genes were identified via integration of betweenness centrality values greater than 100 using CytoHubba. Kyoto Encyclopedia of Genes and Genomes (KEGG) enrichment analysis revealed several significantly affected signaling pathways including the HIF-1, AGE-RAGE (in diabetic complications), IL-17, rheumatoid arthritis and TNF pathways. Integrated-omics and network pharmacology approaches revealed a necessity for further detailed investigation focusing on two major targets, namely NOS2 and NOS3, along with their essential metabolite (arginine) and associated pathways (HIF-1 signaling and arginine and proline metabolism). Real-time PCR validated significantly greater downregulation of NOS2 and HIF-1α in the MJD as compared to the model group. Molecular docking analysis further confirmed the binding of active MJD with key active components. Our findings elucidate the impact of MJD on relevant pathophysiological and metabolic networks relevant to KOA and assess the drug efficacy of MJD and its underlying mechanisms of action.

* Corresponding author. Department of Orthopedics, China.
  E-mail addresses: gk2735@gzucm.edu.cn (K. Gao), 1025517047@qq.com (Z. Huang), yuweiji888@sina.com (W. Yu), ewuyihong@qq.com (Y. Wu), weitty427@163.com (W. Liu), ck0269@163.com (S. Sun), zhangong_9@qq.com (Y. Zhang), 2965393967@qq.com (D. Chen).
  [1] The authors contributed equally to this work.

1. Introduction

Knee osteoarthritis (KOA) is a chronic degenerative joint disease that causes stiffness, pain, and loss of joint function, resulting in damage to articular cartilage and surrounding tissues [1]. Several factors contribute to the development of KOA including aging, obesity, inflammation, trauma, and genetic susceptibility [2]. The prevalence of osteoarthritis is particularly high among the middle-aged and elderly population, with more than 50 % of individuals aged 65 years or more suffering this condition [3].

Despite the availability of several treatments for KOA, a definitive cure remains elusive. Early-stage KOA may offer a potential opportunity to intervene in the disease progression during its initial phases and restore joint homeostasis [4]. The early manifestation of KOA is mainly synovial inflammation and chondrocyte-mediated inflammation [5]. Therefore, effective inhibition of early inflammation might be an important strategy for slowing KOA pathology. Conventional treatment for KOA typically includes administration of oral non-steroidal anti-inflammatory drugs or analgesics, as well as local corticosteroid hormone injections or viscosupplementation, aiming to alleviate pain and enhance joint function. However, such treatments are associated with adverse effects, including an increased risk of upper gastrointestinal symptoms as well as cerebral hemorrhage, kidney disease, and cardio-vascular disease [6].

Traditional Chinese medicine (TCM) has a long history of use in the treatment of joint diseases and has been found effective for relieving pain, reducing inflammation, and improving joint function in patients with osteoarthritis [7]. Juanbi decoction (JBD), a herbal formula recorded in "Yixue Xinwu" by Cheng Zhongling during the Qing Dynasty, exhibits therapeutic effects in dispelling wind and cold, eliminating dampness, and clearing collaterals. It is prepared using a decoction of 12 herbs, namely Qianghuo (Notopterygii Rhizoma Et Radix), Sangzhi (Ramulus Mori), Muxiang (Aucklandiae Radix), Danggui (Angelicae Sinensis Radix), Chuanxiong (Chuanxiong Rhizoma), Duhuo (Radix Angelicae Biseratae), Guizhi (Cinnamomi Ramulus), Gancao (licorice), Ruxiang (Olibanun), Chuanniuxi (Cyathulae Radix), Qinjiao (Gentiana Macrophylla Pall) and Haifengteng (Caulis Piperis Kadsurae). Clinical reports have reported that JBD mitigates intra-articular inflammation, thereby alleviating joint pain and improving functional outcomes in rheumatoid arthritis patients [8]. Furthermore, JBD has demonstrated promising therapeutic effects in the setting of collagen-induced arthritis and rheumatoid arthritis models. It has been found to inhibit autophagy, apoptosis, and proliferation in a collagen-induced arthritis rat model [9,10]. In our clinical practice, modified Juanbi decoction (MJD) was observed to effectively alleviate knee pain and stiffness as well as enhance knee functionality among KOA patients. However, the molecular mechanisms of MJD remain unclear.

Network pharmacology offers an alternative systems-level approach for identifying novel drug candidates that diverges from the conventional focus on individual disease-causing genes or single-target drugs. Instead, it encompasses the entire drug-disease network to discover multi-target drugs with minimum side effects [11]. However, this field is constrained by a singular computational methodology reliant on public databases, limiting its predictive capacity for compound-target combinations and pathway analyses [12]. Meanwhile, traditional metabolomics solely captures end-stage variations in disease and treatments without elucidating the underlying mechanisms of metabolite changes such as relevant biosynthesis pathways and associated proteins [13]. The integration of metabolomics and network pharmacology can be used to employ non-targeted metabolomics methods to assess the impact of compounds such as MJD on pathologies such as KOA and identify crucial metabolites. Subsequently, network pharmacological analysis can be conducted to investigate relevant regulatory proteins and reactions as well as targets affected by MJD. This approach effectively addresses the lack of experimental verification in network pharmacology while compensating for the limited ability of metabolomics to explore upstream molecular mechanisms. As such, the integration of network pharmacology and metabolomics offers a robust approach to scientifically elucidate the metabolic mechanisms of TCM in KOA treatment. In this study, we aimed to identify the active ingredients and molecular targets of MJD, as well as relevant signaling pathways involved in its therapeutic effects. Our results provide valuable insight into the mechanism of action of MJD and provide a foundation for developing more effective treatments for KOA.

2. Experimental materials and methods

2.1. Preparation of MJD

The components of MJD utilized for the experiment were as follows: Qianghuo (60 g), Sangzhi (180 g), Muxiang (48 g), Danggui (180 g), Chuanxiong (42 g), Duhuo (60 g), Guizhi (30 g), Gancao (30 g), Ruxiang (48 g), Chuanniuxi (60 g), and Qinjiao (60 g), Haifengteng (120 g). The herbal extracts utilized in this study were obtained from Kangmei Pharmaceutical Co. (China). To prepare extracts, a mixture of the specified ratio was powdered and then subjected to two rounds of extraction with 10 times the volume of distilled water for a duration of 1.5 h each. The residual material was filtered through multi-layer gauze and the two extracts were combined, concentrated, lyophilized into powder form, and stored at 4 °C for future use.

2.2. Chemoprofile of MJD

The chemical composition and biological activity of MJD samples were assessed using a Waters SYNAPT G2-Si QTOF high-resolution mass spectrometry system and UNIFI quantification software. For analysis, a 100 mg sample was placed in a 15 mL centrifuge tube and treated with a 50:50 (v:v) solution of methanol and water (10 mL). The mixture was sonicated for 30 min. Subsequently, a 1 mL aliquot of the supernatant was centrifuged at 14000 rpm for 5 min, and the resulting supernatant was filtered through a 0.22 μm microporous membrane in preparation for UHPLC-MS/MS analysis. Control samples underwent a similar procedure. The liquid phase conditions for analysis were as follows: column, ACQUITY UPLC HSS T3 (2.1 × 100 mm, 1.8 μm); column

temperature, 35 °C; injection volume, 10 μL; flow rate, 0.25 mL/min; mobile phase, A (deionized water with 0.1 % formic acid) and B (acetonitrile with 0.1 % formic acid); gradient elution.

2.3. 2.3animal experimentation

A cohort of 24 male Sprague-Dawley rats, aged 6–8 weeks, were obtained from Zhuhai Baixitong Biotechnology Co. (Certificate number: SCXK (Guangzhou) 2020-0051). The rats were acclimated to laboratory conditions with a controlled room temperature of 24 $\pm$ 2 °C and a 12-h light/dark cycle for 1 week. Rats were housed in specific pathogen-free facilities and provided with ad libitum access to food. After acclimation, the rats were randomly allocated into a normal control, model or MJD groups (n = 8 rats per group). All groups were subsequently randomly subdivided into two time interval treatment groups of 14 or 28 days, with an equal number of rats per group (n = 4 rats each). The rats in model and MJD groups underwent anterior cruciate ligament transection on their right hind limb to create a rat model of osteoarthritis. The normal control group underwent a sham operation on their right hind limb, which involved an incision and joint cavity wash with normal saline followed by suturing. On the second day after surgery, rats in the MJD group were orally administered MJD (0.3 g/ml per rat) via gavage, whereas both the normal control and model groups were administered an equivalent volume of normal saline orally. All animal experiments were approved by the Animal Welfare and Ethics Committee of Shenzhen PKU-HKUST Medical Center, Shenzhen, China (Approval No. 2023-776).

2.4. Behavioral evaluation

To assess pain behavior among rats, knee circumference, mechanical withdrawal threshold (MWT) and thermal withdrawal latency (TWL) tests were conducted. The von Frey test, described by Chaplan et al. (1994), was used to measure MWT, while a Plantar Test apparatus obtained from UgoBasile, Italy, was employed to measure TWL [14].

Prior to testing, rats were allowed a 30-min acclimation period in elevated plastic cages with wire mesh bases. Testing involved multiple trials on both left and right hindpaws using the von Frey needle and focused radiant heat, respectively. A positive response, characterized by a rapid withdrawal of the paw and paw licking, was noted in each trial. The thermal hyperalgesia test did not exceed 20 s in duration.

2.5. Histopathological analyses

Rat joints were immobilized and decalcified following rat sacrifice. Subsequently, samples were embedded in paraffin, sectioned to a 2–3 μm thickness, and stained with a variety of dyes including HE (hematoxylin and eosin) and S&O (Safranin O/Fast green). Osteoarthritis progression was evaluated according to the Mankin scoring system.

2.6. Micro-CT analysis

Knee joint samples from each rat group were fixed with a 40 g/L paraformaldehyde solution. The entire knee joint, including 5 mm of both the tibia and femur, was scanned using micro-CT (X-ray tube voltage: 70 kV; current: 114 μA; exposure time: 1180 ms). A total of 30 consecutive sections were scanned for each sample. Resulting data were analyzed using the accompanying software and measurements of bone mineral density and relative bone volume fraction (bone volume/trabecular volume, BV/TV) values in the corresponding regions were performed. The micro-CT scanning regions of interest included the subchondral bone plate and the subchondral trabecular bone.

2.7. LC-Q-TOF-MS analysis

The LC-Q-TOF-MS analysis was performed by combining liquid chromatography and mass spectrometry techniques. After preparation (which included centrifugation, concentration and reconstitution), samples were analyzed using an ACQUITY UPLC® HSS T3 column. Gradient elution was employed with different mobile phases for positive and negative ion modes. Mass-spectrometric detection was performed using an Orbitrap Exploris 120 instrument with an ESI ion source. The acquired data included MS1 and MS/MS spectra. Experimental parameters such as gas pressure, spray voltage, temperature and collision energy were optimized.

2.8. Multivariate analysis of serum metabolic profiles and biomarker identification

The LC-Q-TOF-MS data were processed using XCMS for feature detection, retention time correction and alignment. Metabolite identification was performed by matching accurate mass and MS/MS data with various databases. Data normalization was performed using the QC-RLSC method and ion peaks with RSDs >30 % in QC samples were excluded. Multivariate data analysis was performed using the ropls R package and included PCA, PLS-DA and OPLS-DA modeling. Permutation tests assessed model overfitting and model performance was evaluated using R2X, R2Y and Q2 values. Discriminating metabolites were determined based on P-values, FC, and VIP values. Pathway analysis was performed using MetaboAnalyst by mapping metabolites to Kyoto Encyclopedia of Genes and Genomes (KEGG) pathways for further interpretation. Visualizations were generated using the KEGG Mapper tool.

2.9. Network pharmacological analysis

Active compounds were identified from reliable sources and screening was performed based on bioavailability and drug-like activity criteria. Targets were predicted using SEAware software and validated using databases like Genecards and DisGeNET. Protein-protein interactions were analyzed using Cytoscape, thereby facilitating network construction. Gene ontology (GO) annotation and KEGG pathway enrichment analyses were performed using the DAVID (https://david.ncifcrf.gov/) database to uncover molecular mechanisms. These analyses provided insights into the therapeutic effects of MJD on OA.

2.10. Molecular docking

Selected key genes were assessed for molecular docking with the core components of MJD. Initially, 2D structures of the active MJD components were downloaded from the PubChem database. These structures were saved in the ".sdf" format. Open Babel software was utilized to evaluate structures and optimize their mechanical properties. Subsequently, optimized structures were saved in the ".mol2″ format. Target protein crystal structure was obtained from the RCSB protein database (https://www.rcsb.org/). Protein structure was retrieved in the ".pdb" format. Both the ligand and receptor files were converted to the ".pdbqt" format using AutoDockTools 1.5.7. During this process, water molecules were removed and hydrogen atoms were added to replace them. Python 3.7.9 was used for molecular docking analysis. Python scripts were written to perform the molecular docking analysis, utilizing the prepared ligand and receptor files in ".pdbqt" format. Docking results were analyzed and visualized using appropriate tools and libraries.

2.11. Real-time PCR

To extract RNA, rat knee joints from all groups were immediately immersed in liquid nitrogen after dissection. Subsequently, the samples were pulverized using a mortar and pestle. Total RNA was extracted from knee joints using TRIzol reagent according to the manufacturer's protocol (Invitrogen). The RNA was then converted into complementary DNA (cDNA) using SuperScript II reverse transcriptase. Real-time PCR was performed using the StepOnePlus Real-Time PCR System and SYBR Green PCR Master Mix (Applied Biosystems by Life Technologies, 4367659). The β-Actin reference gene was employed for signal normalization and relative gene expression was calculated using the $\Delta\Delta CT$ method. To validate finding reliability, these procedures were repeated three times.

2.12. Statistical analyses

Data were presented as mean ± standard error values obtained from three independent experiments. Statistical comparisons were
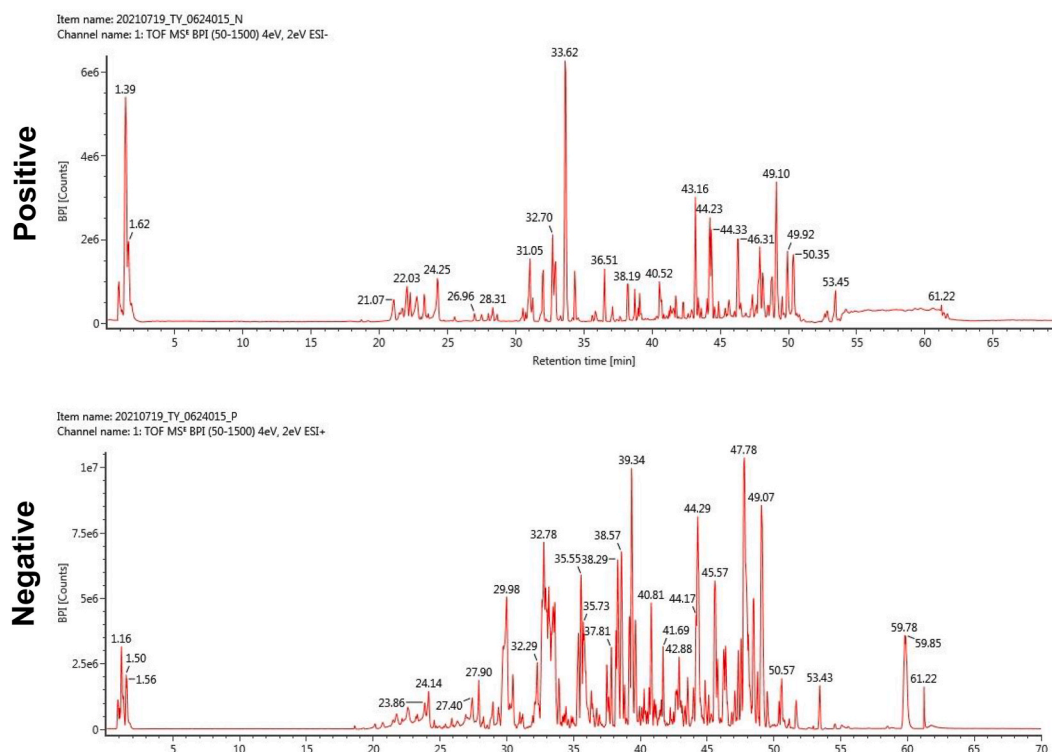

Fig. 1. Total ion chromatogram of UPLC/MS/MS analysis in positive and negative ion modes.

performed using GraphPad Prism 7.0 software. The significance of differences was determined using either the *t*-test or one-way analysis of variance (ANOVA). A P-value less than 0.05 or 0.01 was considered statistically significant.

3. Results

3.1. The MJD chemoprofile

Here, we utilized a Waters SYNAPT G2-Si Qt high-resolution mass spectrometry system and UNIFI software to analyze the chemical composition of MJD. UNIFI software is designed to manage the diverse needs of acquiring, processing, reporting, storing and providing permission-based access to complex scientific information generated by UPLC/MS and UPLC/MS/MS systems. The total ion chromatogram of MJD in positive and negative ion modes is illustrated in Fig. 1.UPLC I-Class and SYNAPT G2-Si Qt were employed for chromatographic separation and mass spectrometry of the chemical components of MJD. The theoretical mass spectrometry database of 6400 natural product components was processed using UNIFI, resulting in the identification of 228 components (Supplementary Table 1). Detected compounds were ranked based on mass spectrum response values. The activity data for the top 20 compounds with highest response rates are presented in Table 1.

3.2. Therapeutic effects of MJD on a rat model of early KOA

A rat model of KOA was established to evaluate the therapeutic effects of MJD. Changes in knee circumference, MWT and TWL were investigated. As shown in Fig. 2A, rats in the 14-day MJD group exhibited a smaller knee circumference as compared to the model group ($P < 0.01$). The MWT and TWL of the 14-day MJD group were significantly decreased as compared to the model group (both $P < 0.01$) (Fig. 2B and C). The circumference of the knee serves as an indicator of joint swelling, while MWT and TWL reflect the level of joint pain. The aforementioned changes demonstrate that MJD effectively alleviated both joint swelling and pain in KOA rats following a 14-day intragastric administration regimen. Moreover, numerous subsequent pathological analyses were performed on specimens collected at the 14-day time point.

3.3. In vivo chondroprotective effects of MJD on a rat model of early KOA

Histopathological changes in articular cartilage were assessed using HE and SO-FG staining as well as micro-CT imaging, as illustrated in Fig. 3A. The HE staining revealed that in the control group, the cartilage layer was substantially thickened with numerous chondrocytes that were normally arranged and distributed. The chondrocytes appeared round or oval-shaped, with centrally located nuclei, complete cytoplasmic content and intact morphology. In contrast, the model group was found to have a thin cartilaginous layer characterized by a reduced quantity of vacuolar chondrocytes. Additionally, disordered arrangement of cells across all layers along with scattered clusters was noted. Comparatively, the MJD group demonstrated a relatively flat cartilage surface with an increased thickness of the cartilage layer and a higher number of normal chondrocytes. The MJD group exhibited improved morphology of articular cartilage. Uniform SO-FG staining of cartilage layer was noted among control group rats. Among model group rats, safranin depletion was noted on the superficial surface of articular cartilage, indicating significant loss of proteoglycan and a presence of cartilage surface irregularities. The micro-CT analysis revealed that the subchondral bone trabeculae in the control group exhibited a uniform, regular shape and an orderly arrangement. In contrast, the model group exhibited subchondral trabecular broadening and

Table 1
The activity data for the top 20 compounds in MJD with highest response.

| Name	Molecular Formula	Molecular Weight	Retention Time	Peak Area	Relative Abundance/%
Pachymaric acid AM	C32H48O5	512.4	47.8	8287140	13.768
(−)- olivine	C20H24O7	376.2	32.8	5538817	9.202
South schisandrin acid	C30H46O4	470.3	44.3	4267919	7.091
Angelicol A	C20H24O7	376.2	33.2	4029125	6.694
Glycyrrhizic acid	C42H62O16	822.4	33.6	2298273	3.818
Ganoderma F	C30H46O3	454.3	44.2	1930619	3.208
Kuwanon C	C25H26O6	422.2	38.2	1114364	1.851
Kirenol	C20H34O4	338.2	35.6	1095624	1.820
Hawthorn D	C23H20O10	456.1	1.4	1074783	1.786
Epianhydrobelachinal	C30H44O4	468.3	41.7	907467	1.508
Ferutosterone A	C24H28O4	380.2	42.7	678833	1.128
Quassitol A	C24H36O7	436.2	50.6	651850	1.083
3-Epioleanolic acid	C30H48O3	456.4	48.8	646793	1.075
Betulonic acid	C30H46O3	454.3	49.1	636980	1.058
LucialdehydeA	C30H46O2	438.3	48.1	603428	1.003
Ganoderma B	C30H46O4	470.3	46.2	531987	0.884
2 alpha-hydroxyursolic acid	C30H48O4	472.4	44.2	529957	0.880
23-hydroxybetulinic acid	C30H48O4	472.4	46.3	454154	0.755
Dihydrocoumarin	C9H8O2	148.1	22.6	446165	0.741
3β,16α-dihydroxylanostere-7,9(11), 24-triene-21-acid	C30H46O4	470.3	40.7	445502	0.740
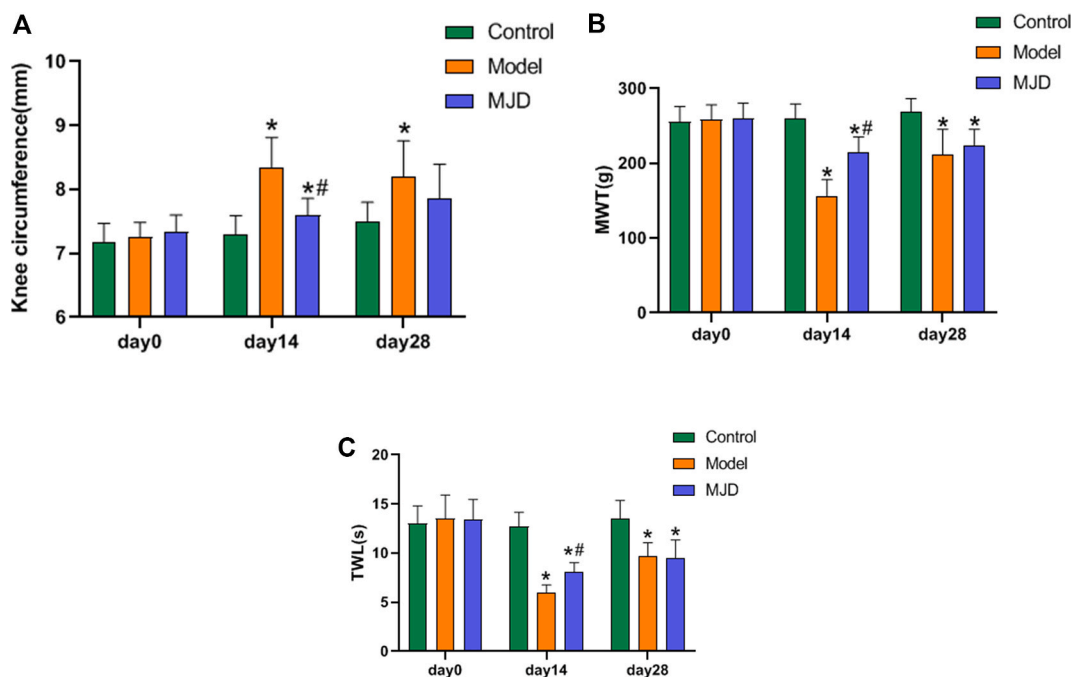
Fig. 2. Knee circumference (A), MWT (B) and TWL (C) results of the hind paws of rats tested before KOA modeling (0 day) and after final MJD treatment (28 d). Values are presented as mean ± SD. *P < 0.01 vs. Control group; #P < 0.01 vs. Model group.

osseodensification along with disordered and unevenly trabecular arrangement. Moreover, the reticular structure was absent, and varying degrees of oval or round osteophytes were formed at the medial edge of the joint. As compared to model group rats, those of the MJD group exhibited a more uniform distribution of subchondral bone trabeculae with regular shapes and an orderly arrangement.

The Mankin score is a standardized measure for assessing the extent of cartilage degeneration in osteoarthritis [15]. Model group exhibited a significantly higher Mankin score as compared to the control group ($P < 0.01$); while the MJD group exhibited a significantly decreased Mankin score as compared to the model group ($P < 0.01$), as shown in Fig. 3B.

The pathological features of osteoarthritis encompass cartilage degeneration, synovial inflammation and subchondral bone remodeling (demonstrated to precede other pathological processes) [16]. Cartilage health is contingent upon the mechanical state of subchondral bone. Subchondral bone remodeling results in loss of bone mass, affecting not only the subchondral bone plate but also cancellous bone density, including bone mineral density (BMD), trabecular number (TB.N), and trabecular thickness (TB.Th). As shown in Fig. 3C-E, the model group exhibited significantly lower bone mineral density, trabecular number and trabecular thickness as compared to the control group ($P < 0.01$). In contrast, the MJD group exhibited significantly increased bone mineral density, trabecular thickness and trabecular number as compared to the model group ($P < 0.01$). The aforementioned findings demonstrate that MJD enhanced subchondral bone mass and biomechanical properties of subchondral bone in rats with KOA.

3.4. Serum metabolomics analysis

In order to gain insight into the metabolic effects of MJD on KOA pathology, we conducted a comprehensive analysis of differential metabolites in serum samples obtained from rats. During initial data analysis, UPLC-Triple TOF ESI (+) and ESI (−) total ion chromatography of quality control samples were found to exhibit well-defined peaks and a relatively uniform distribution under test conditions. PCA analysis of quality control data further confirmed system stability and result reproducibility (Supplementary Fig. 1). Subsequently, PLS-DA and OPLS-DA were employed to demonstrate significant separation between MJD and model group rats (Fig. 4A1-2).

Utilizing a OPLS-DA model that considered a VIP>1 and a $P < 0.05$, we identified a total of 33 differentiated metabolite ions. Among them, 15 ions were upregulated (fold change >1) while 18 ions were downregulated (fold change <1) in the MJD group. This suggests that MJD partially restored metabolite dysregulation associated with osteoarthritis (Supplementary Table 2). Heat maps were generated to visualize metabolite variations between the two groups (Fig. 4B), revealing that all candidate metabolites exhibited alterations in the model group, with the majority of results inversed in the MJD group. To further explore the metabolic pathways influenced by MJD in KOA rats, we imported all differential metabolites into MetaboAnalyst 5.0 (Fig. 4C). This analysis highlighted several significantly affected pathways, namely arginine and proline metabolism, vitamin B6 metabolism, as well as phenylalanine, tyrosine and tryptophan biosynthesis. Metabolites associated with these pathways included L-arginine, gamma-aminobutyric acid, *cis*-4-hydroxy-D-proline, 4-acetamidobutanoic acid, pyridoxamine, 4-pyridoxic acid and L-tyrosine.
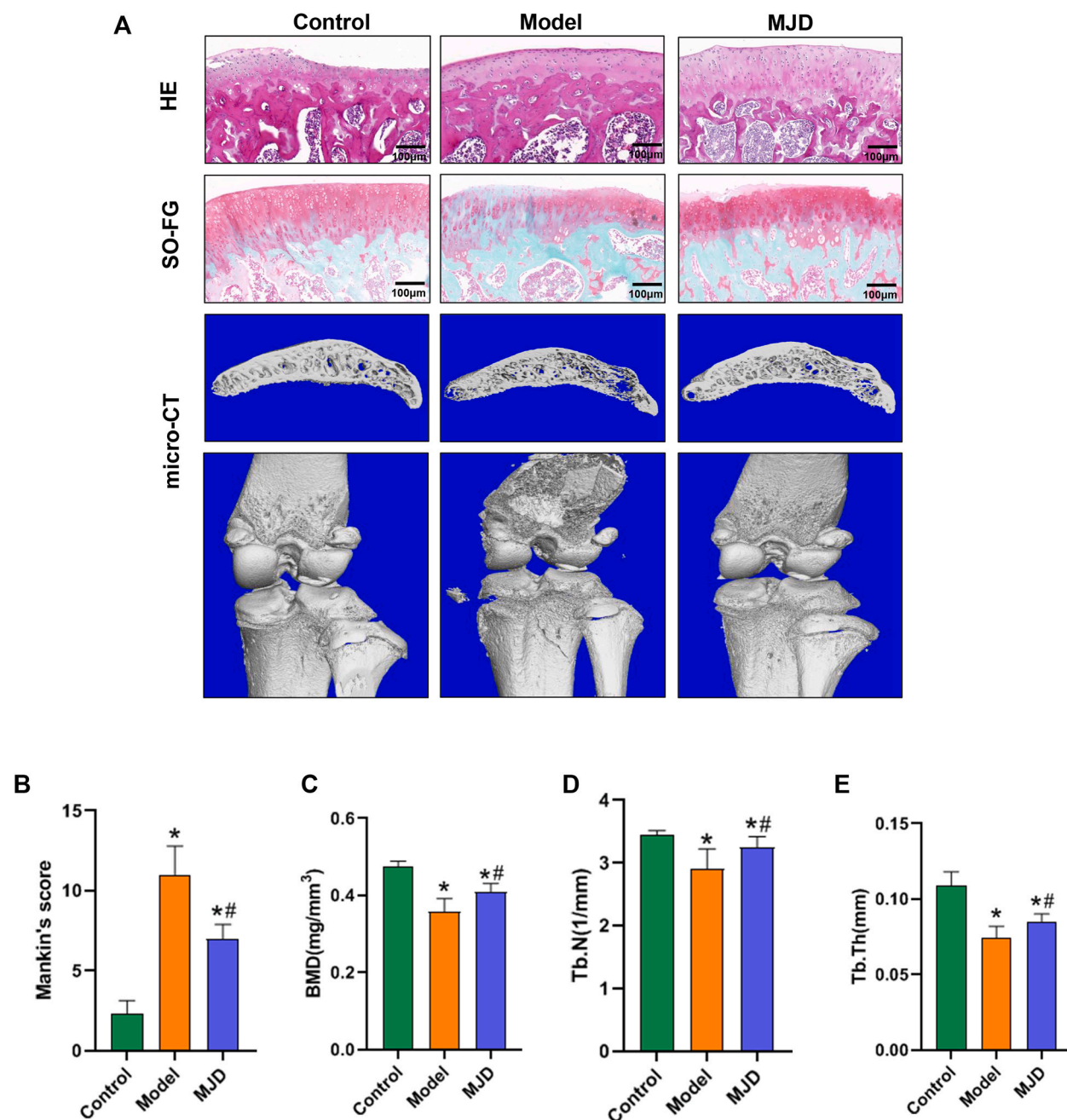
Fig. 3. Protection of different administration groups on KOA rats. (A) Representative histological staining and safranin O/fast green staining and micro-CT scanning of the knee joint of different groups. (B) Statistical analysis of Mankin's scoresfor histopathological observation. (C) quantitative statistics of bone density, (D) trabecular number, (E) trabecular thickness. Values are presented as mean ± SD. *P < 0.01 vs. Control group; #P < 0.01 vs. Model group.

3.5. Network pharmacology of potential compound-target pathways

To understand the complex interplay of multiple components, targets and pathways relevant to the therapeutic effects of MJD in the setting of KOA, we performed a network pharmacology analysis. Initially, extensive searches in the TCMSP (https://old.tcmsp-e.com/tcmsp.php), TCMID (https://ngdc.cncb.ac.cn/databasecommons/database/id/437) and TCM_Taiwan (http://tcm.cmu.edu.tw/) databases identified a total of 1027 compounds present in MJD (Supplementary Table 3). Subsequently, 1637 genes were extracted from the SEA Search Server (https://sea.bkslab.org/) database while 862 genes associated with osteoarthritis were extracted from the GeneCards (https://www.genecards.org/) and DisGeNET (https://www.disgenet.org/home/) databases. Comparative analysis
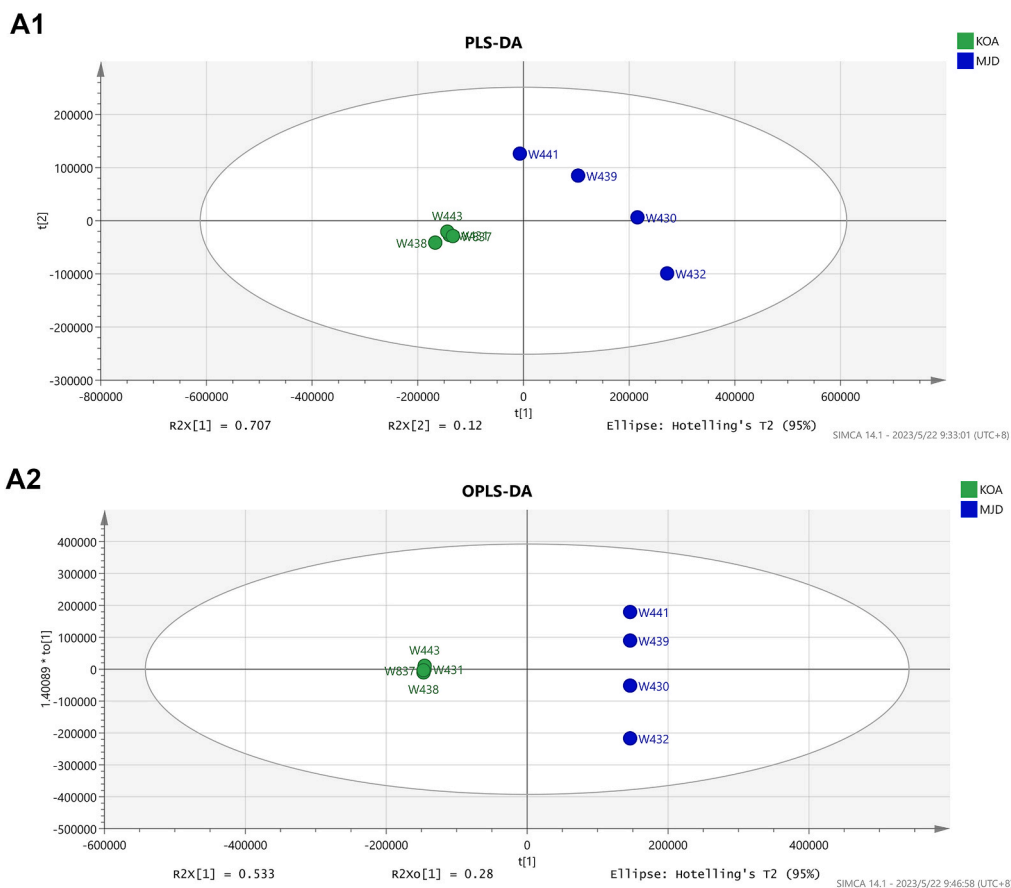
Fig. 4. Differential metabolites in serum were identified between the MJD group and the KOA group. (A) PLS-DA and OPLS-DA score plots of the MJD on the KOA rat; (B) A total of 15 upregulated and 18 downregulated metabolite ions were displayed in the heatmap with VIP > 1 and P < 0.05. (C) The KEGG enrichment analysis of the detailed pathways in which differential metabolites played a role.

revealed that 140 dysregulated genes overlapped with the molecular targets of MJD (Fig. 5A). To identify hub genes targeted by MJD relevant in osteoarthritis, we constructed a protein-protein interaction (PPI) network (https://cn.string-db.org/) using Cytoscape 3.7.2. Fig. 5B provides an overview of the relationships among the 140 targets (with the exception of 5 unrelated genes). Hub genes were determined using CytoHubba and combined with our calculated score. Betweenness centrality refers to the count of shortest paths connecting nodes within a network. A higher betweenness centrality indicates an increased number of pathways. This metric is useful in identifying crucial regions that act as bridges between different subnetworks [17]. In this study, the 39 genes with a betweenness centrality value greater than 100 were designated as hub genes based on calculated median and mean values (Supplementary Table 4).

To uncover the functions of potential targets, we performed GO and KEGG pathway enrichment analyses using the DAVID (https://david.ncifcrf.gov/) database. The top terms identified on GO analysis included wound healing involved in the inflammatory response (GO:0002246), vascular endothelial growth factor production (GO:0010573), arginine catabolism (GO:0006527), nitric-oxide synthase activity (GO:0004517) and arginine binding (GO:0034618), as shown in Fig. 5C. KEGG enrichment analysis revealed several affected signaling pathways, namely the HIF-1, AGE-RAGE (in diabetic complications), IL-17, rheumatoid arthritis and TNF pathways (Fig. 5D).

3.6. Integration of metabolomics and network pharmacology analyses

To gain a comprehensive understanding of the mechanisms underlying the effects of MJD in the setting of KOA, we performed an integrated analysis combining metabolomics and network pharmacology. Differential metabolites identified were utilized to construct compound-reaction-enzyme-gene networks using the MetScape plugin in Cytoscape, as showed in Fig. 6. By matching potential targets obtained from network pharmacology with genes in the MetScape analysis, we identified NOS2 and NOS3 as key targets. The key metabolite associated with these targets was ʟ-arginine, and the affected pathway was arginine and proline metabolism. These findings suggest that NOS2 and NOS3, along with the related metabolite ʟ-arginine, play crucial roles in the therapeutic effects of MJD in the
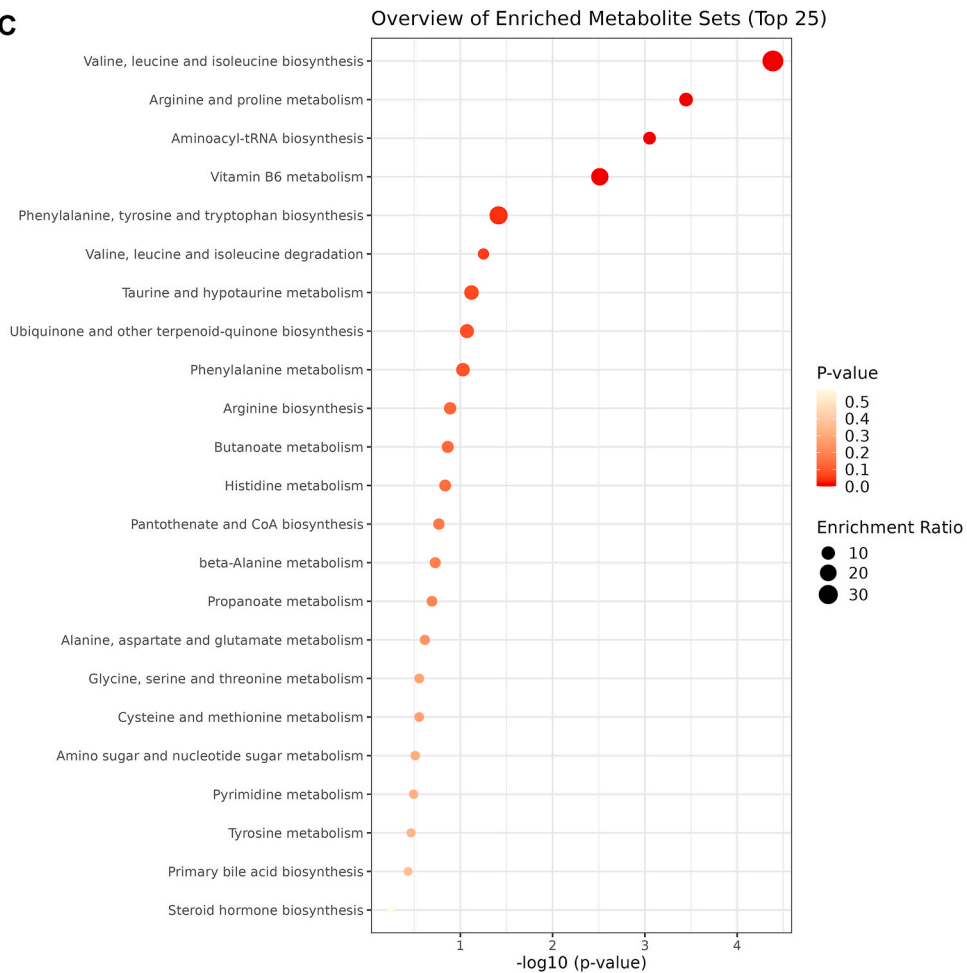
B

C

Overview of Enriched Metabolite Sets (Top 25)
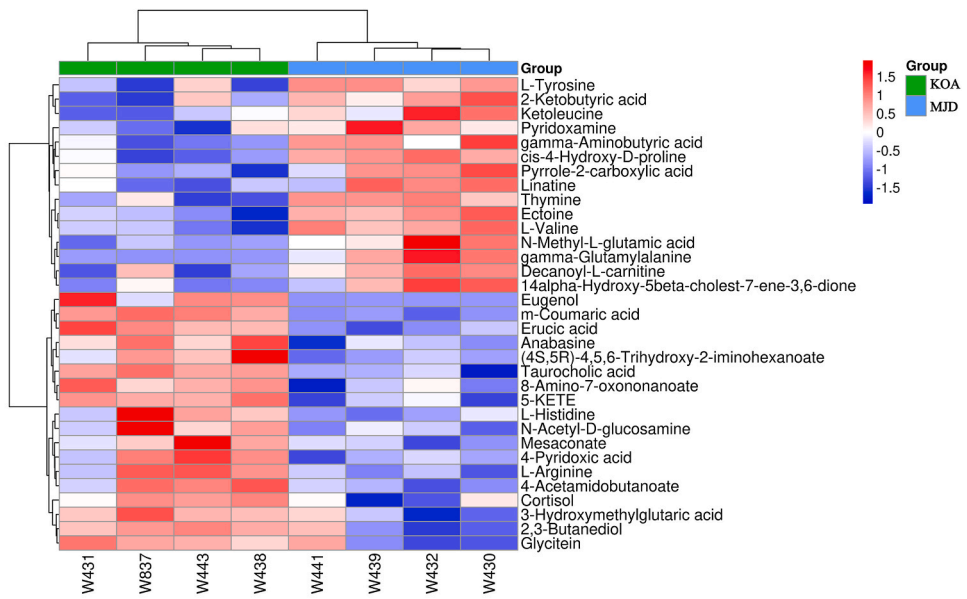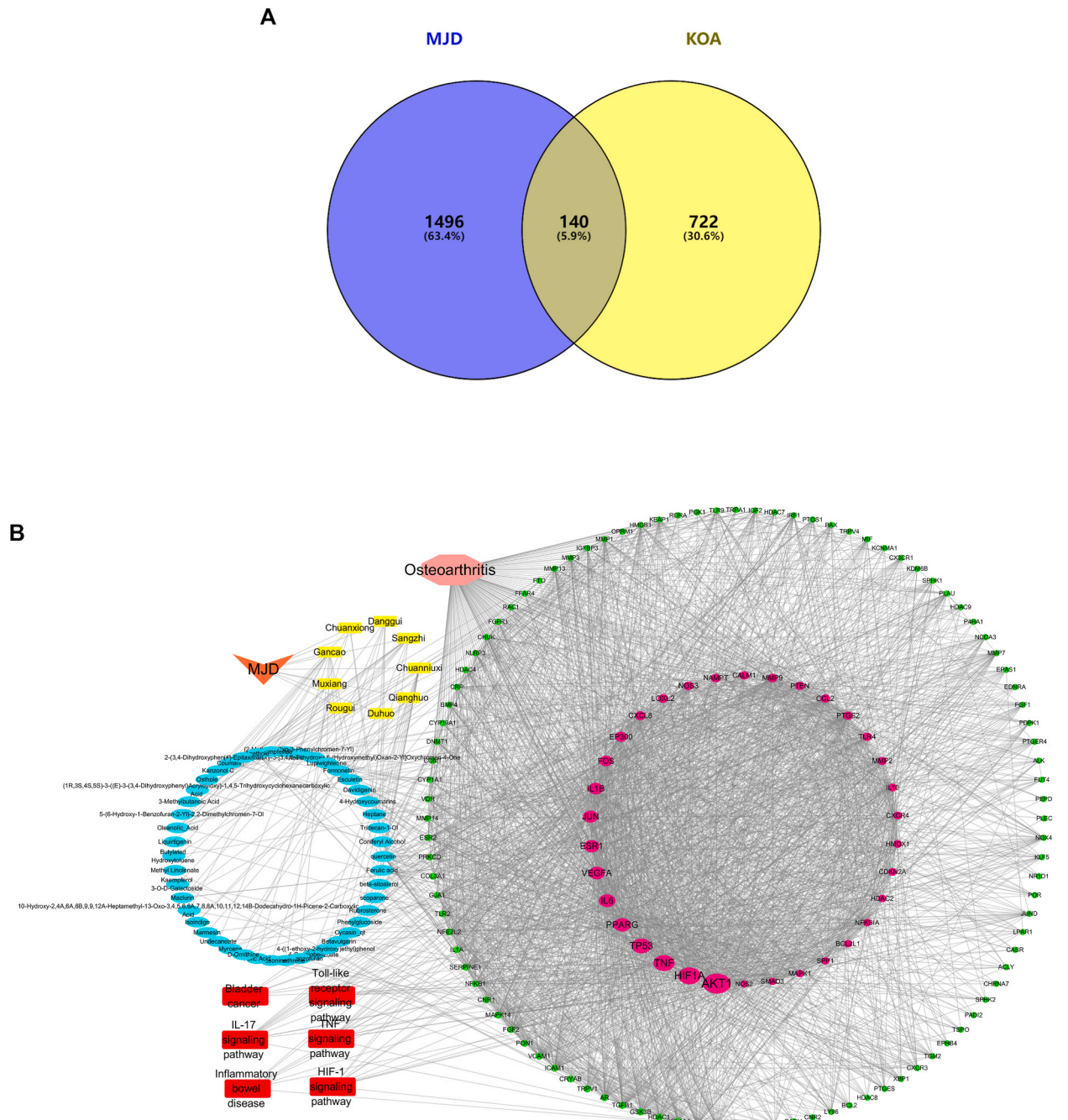
Fig. 4. (*continued*).

Fig. 5. Network pharmacology predicted the possible herb-compound-target-pathway interaction in MJD mediating the therapeutic effect of KOA. (A) Venn analysis on putative targets of MJD as well as osteoarthritis-related genes. (B) The network illustrated the interaction among main herbs, active components, targeted genes and corresponding pathways. The yellow rectangle indicated the main herb of MJD, while the light-blue oval represented the main compound. The light-red circle indicated the pathway-related target, while the green circle represented the non-pathway-dependent target. Meanwhile, the red rectangle indicated the corresponding pathway. (C) GO enrichment analysis of potential targets. (D) The pathway enrichment analysis was performed related to main herbs.
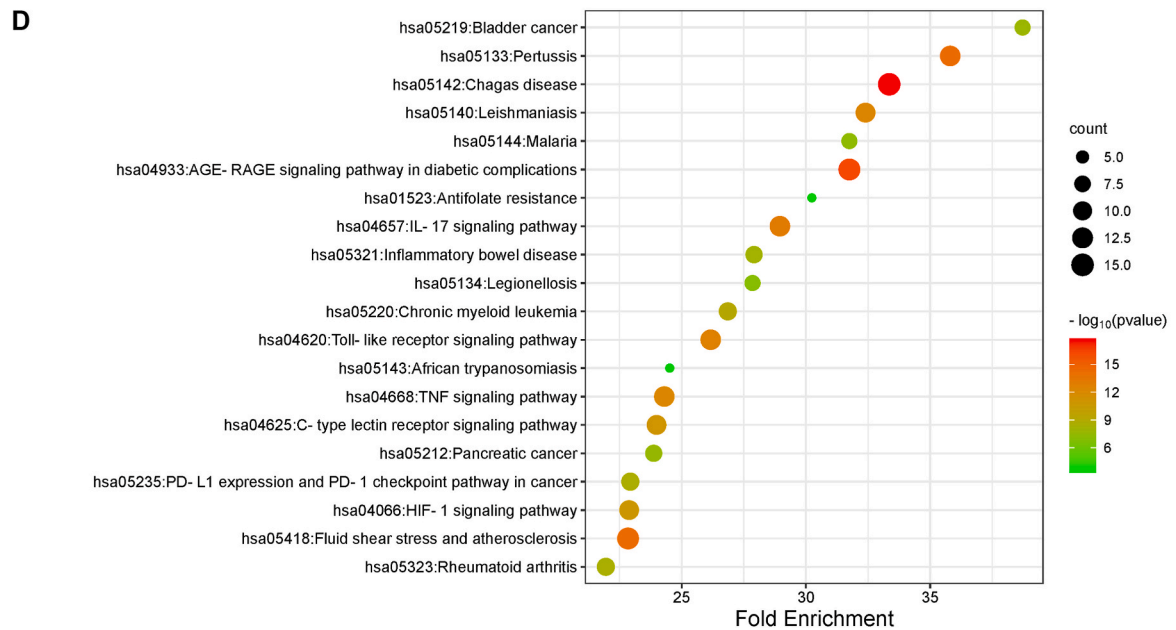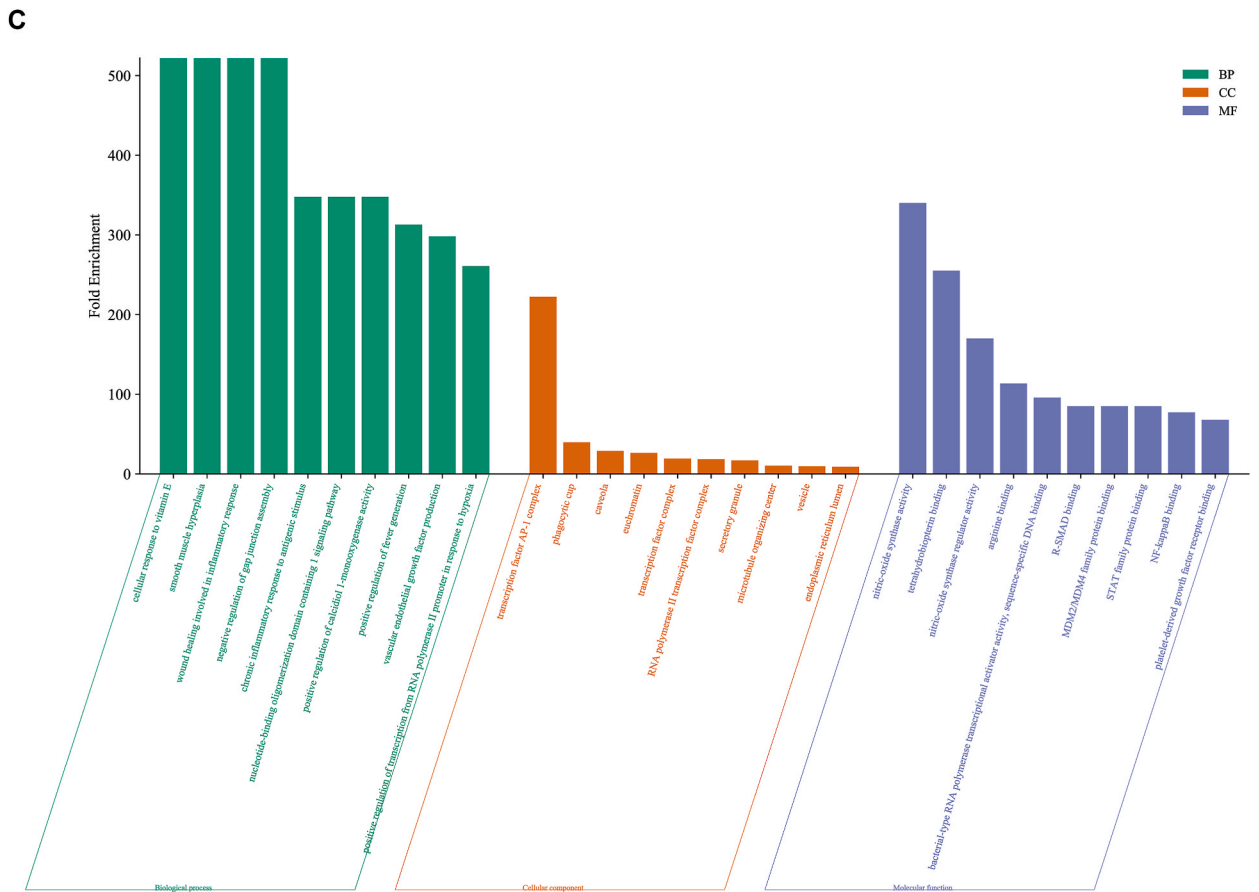
C

D

Fig. 5. (*continued*).

Fig. 6. The compound-reaction-enzyme-gene networks of the key metabolites and targets. The red hexagons, grey diamonds, green round rectangle and purple circles represent the active compounds, reactions, proteins and genes, respectively. The key metabolites, proteins and genes were magnified.

setting of KOA. Notably, we found these two key targets to be specifically involved in HIF-1 signaling, which was previously identified via KEGG enrichment analysis.

3.7. Key gene validation

To validate the expression of HIF-1α and NOS2 in knee joint, we extracted RNA from the rat knee joints in all 14-day time point groups (n = 4 rats each) and performed RT-PCR analysis. Our results revealed that HIF-1α and NOS2 in knee joint exhibited reduced expression in the MJD group as compared to the model group (Fig. 7A and B).

3.8. Molecular docking

Upon searching the RCSB protein database, molecular docking analysis was performed to investigate the probability of interaction among the active components of MJD and key targets. Binding energy was used to assess the strength of interactions between small molecules and proteins. If the binding energy was less than −1.2 kcal mol −1, molecules were considered to possess a high binding activity; smaller values indicated greater binding activity. Based on molecular docking data (Table 2), the binding energies of active
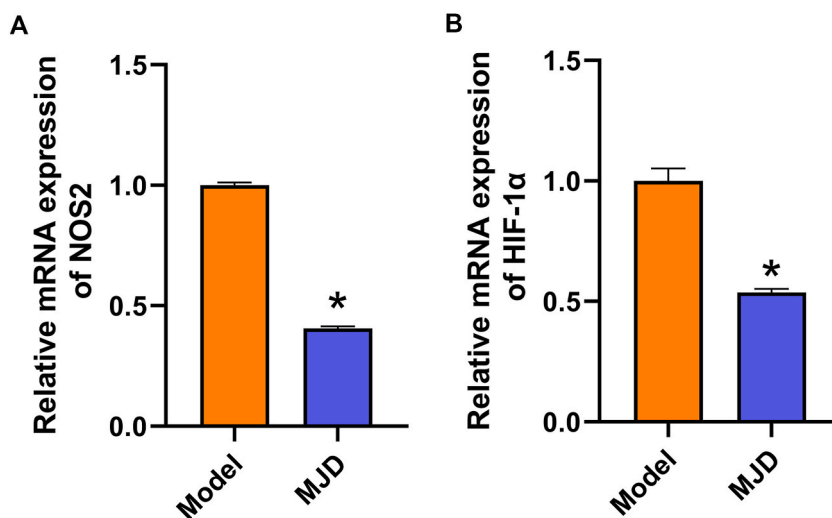
Fig. 7. Relative mRNA expression of HIF-1α and NOS2 in the rat knee joints (n = 4 rats each). (A) The MJD group exhibited significantly lower mRNA NOS2 expression as compared to the model group ($P < 0.01$); (B). The MJD group exhibited significantly lower mRNA HIF-1α expression as compared to the model group ($P < 0.01$). Values are presented as mean ± SD. *$P < 0.01$ vs.Model group.

MJD components with target proteins (AKT1, HIF1A, VEGFA, NOS2, NOS3) was determined, revealing values lower than −1.2 kcal mol −1. Data analysis revealed that the main MJD components (e.g. beta-sitosterol, osthol, quercetin, kanzonol C) favorably bind key targets (AKT1, HIF1A, VEGFA, NOS2 and NOS3). The molecular docking structures of top-ranked complexes are shown in Fig. 8A–D.

4. Discussion

Here, we investigated the therapeutic effects of MJD on a rat model of early KOA to elucidate relevant underlying mechanisms of action. Our findings demonstrated that MJD effectively alleviated swelling and pain in rats with KOA, as evidenced by improvements in knee circumference, MWT and TWL measures. Histopathological changes revealed reduced degenerative manifestations in the articular cartilage of rats treated with MJD as compared to model group rats. Network pharmacology analysis of MJD revealed a total of 39 hub genes and several significantly relevant signaling pathways including the HIF-1, AGE-RAGE (in diabetic complications), IL-17, Toll-like receptor and TNF signaling pathways.

Among relevant hub genes, AKT1, HIF1A, TNF, IL6, VEGFA, IL1B, NOS3, MMP9, PTGS2, NFKB1A, NOS2 and RELA likely exert a crucial influence on the pathogenesis of osteoarthritis. Mechanistically, prolonged activation of Akt signaling causes an accumulation of reactive oxygen species and triggers chondrocyte senescence as well as expression of a senescence-associated secretory phenotype. Disrupted Akt signaling in articular chondrocytes triggers oxidative stress-induced chondrocyte senescence and leads to osteoarthritis [18]. Importantly, hypoxia inducible factor (HIF) -1A plays a pivotal role in maintaining oxygen balance in the setting of hypoxia and exerts a critical influence on chondrocyte survival within knee joint cartilage under hypoxic conditions, thereby ensuring proper physiological functionality and metabolic homeostasis [19]. The pro-inflammatory cytokines tumor necrosis factor α (TNF-α), interleukin-1β (IL-1β), prostaglandin synthase 2 (PTGS2) and interleukin-6 (IL-6) are pivotal in the pathogenesis of osteoarthritis, playing a crucial role in the degradation of articular cartilage [2]. Vascular endothelial growth factor (VEGF) is a potent stimulator of angiogenesis and also contributes to inflammation. VEGF was found to be elevated in the synovial membrane, subchondral bone, synovial fluid, serum and articular cartilage of osteoarthritis patients [20]. Matrix metalloproteinase-9 (MMP-9) is primarily secreted by mononuclear cells and macrophages within articular cartilage. Under the pro-inflammatory conditions of osteoarthritis, there is

Table 2
The binding energy of the MJD components with the target proteins.

| Herb	Active components	Target	Binding energy (kcal/mol)
Chuanniuxi	beta-sitosterol	NOS3	−8.92
Chuanniuxi	beta-sitosterol	VEGFA	−8.16
Duhuo	Osthole	NOS2	−6.6
Chuanniuxi	Quercetin	HIF1A	−6.54
Gancao	Kanzonol C	NOS3	−6
Chuanniuxi	4-((1-ethoxy-2-hydroxy)ethyl)phenol	NOS2	−5.07
Sangzhi	Kaempferol 3-O-D-Galactoside	AKT1	−4.52
Sangzhi	2-(3,4-Dihydroxyphenyl)-5,7-Dihydroxy-3-[3,4,5-Trihydroxy-6-(Hydroxymethyl)Oxan-2-Yl] Oxychromen-4-One	VEGFA	−3.81
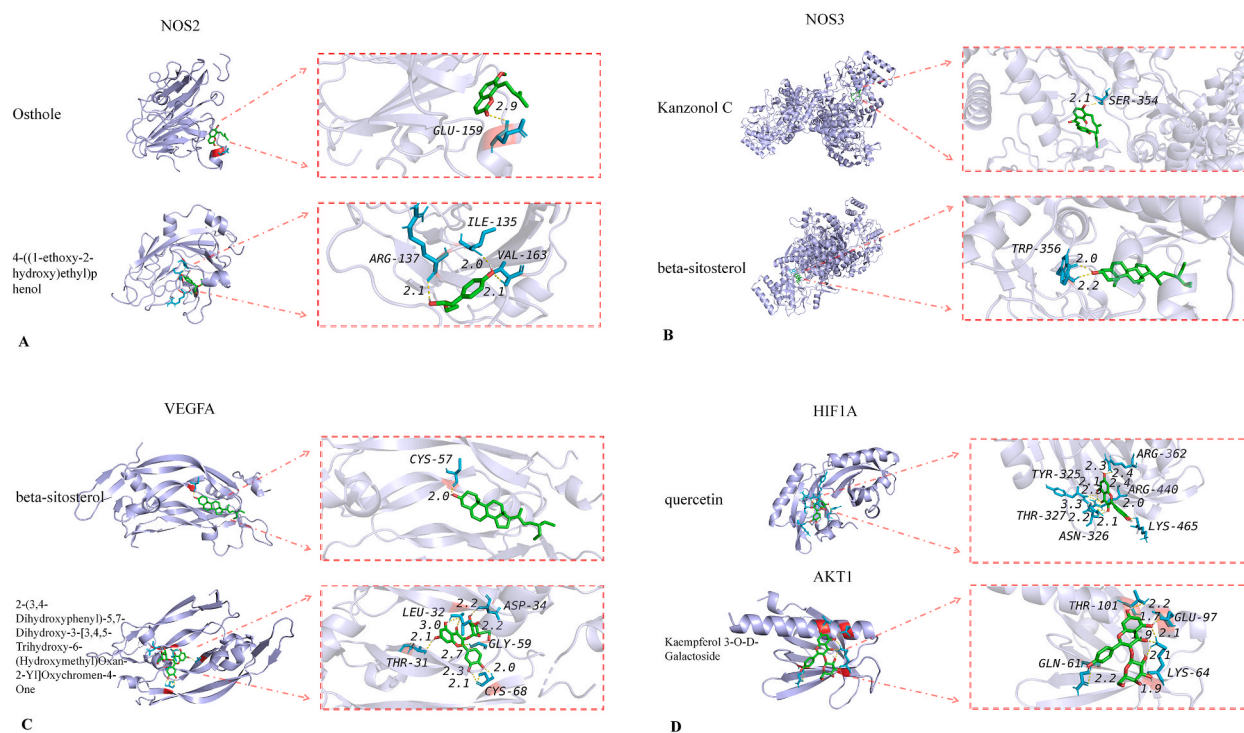
Fig. 8. The 3D interaction diagrams of active drug components and the target proteins by molecular docking. (A) NOS2 protein docked with Osthole and 4-((1-ethoxy-2-hydroxy)ethyl)phenol. (B) NOS3 protein docked with Kanzonol C and beta-sitosterol. (C) VEFA protein docked with beta-sitosterol and 2-(3,4-Dihydroxyphenyl)-5,7-Dihydroxy-3-[3,4,5-Trihydroxy-6-(Hydroxymethyl)Oxan-2-Yl]Oxychromen-4-One. (D) HIF1A protein docked with quercetin and AKT1 protein docked with Kaempferol 3-*O*-D-Galactoside.

enhanced secretion of MMP-9 by macrophages, which in conjunction with other pro-inflammatory mediators accelerates arthritic pathology, facilitates cartilage degeneration and induces excessive subchondral bone growth [21]. In the several pathways significant to this illness, IL-17 signaling pathway was noted to be involved in inflammation and articular cartilage degradation. This occurs via the release of a number of pro-inflammatory mediators, enhancement of neutrophil chemotaxis, induction of nitric oxide synthase (NOS), matrix metalloproteinase production (within cartilage), as well as activation of synovial cell-degrading enzyme activity [22]. The TNF signaling pathway acts as an inflammatory mediator and exerts many biological effects. TNF-α induces IL-6 production and activates the protease that degrades cartilage and synovium [23]. Activation of Toll-like receptor signaling pathway enhances release of inflammatory factors such as IL-1β and TNF-α, activates NF-κB in downstream signaling and induces articular chondrocyte apoptosis [24].

Serum metabolomics analysis was performed to gain insight regarding the metabolic effects of MJD on KOA. Metabolic pathway analysis revealed involvement of several pathways including arginine and proline metabolism, vitamin B6 metabolism, and phenylalanine, tyrosine and tryptophan biosynthesis pathways. Metabolites associated with these pathways included ʟ-arginine, gamma-aminobutyric acid, *cis*-4-hydroxy-ᴅ-proline, 4-acetamidobutanoic acid, pyridoxamine, 4-pyridoxic acid and ʟ-tyrosine. Vitamin B6, which has been reported to mitigate negative effects induced by reactive oxygen species via inhibition of xanthine oxidase activity, was found to exert a protective effect on cartilage by regulating oxidative stress, a pivotal factor implicated in various pathologies including osteoarthritis [25]. ʟ-arginine was demonstrated that ʟ-arginine alleviated arthritis pathology, inflammatory osteoclastogenesis and inflammation-induced bone loss by modulating amino acid metabolism in osteoclasts [26]. Similarly, ʟ-proline plays a vital role in collagen synthesis, which is essential for tendon and joint health. Tyrosine, a nonessential amino acid, is endogenously synthesized via conversion from phenylalanine. Elevated levels of tyrosine in the serum of osteoarthritis patients were previously reported, suggesting that reduction of ʟ-tyrosine levels may confer potential benefits in the management of osteoarthritis [27]. Tryptophan metabolism, primarily occurring via the kynurenine pathway and mediated by intestinal immune and epithelial cells via the enzyme indoleamine 2, 3-dioxygenase, plays a pivotal role in inflammation and neurotransmission [28]. Furthermore, osteoarthritis patients were reported to exhibit significantly lower plasma levels of ʟ-tryptophan as compared to healthy controls, thereby suggesting that enhancing ʟ-tryptophan concentrations may confer potential benefits in this patient population [29].

To gain a comprehensive understanding of the mechanisms underlying the effects of MJD in the setting of KOA, we performed an integrated analysis combining metabolomics and network pharmacology, followed by construction of a compound-reaction-enzyme-gene network. We found NOS2 and NOS3, along with the arginine and proline metabolism pathways, to play crucial roles in the therapeutic effects of MJD on KOA rats. Moreover, HIF-1 signaling pathway was found to closely associate with effects exerted by MJD. One of the key mediators involved in the pathogenesis of osteoarthritis is nitric oxide (NO), which is produced by NOS [30]. Moreover,

inducible (NOS2) and endothelial (NOS3) NOS have been implicated in cartilage degeneration and synovial inflammation [31–33]. Importantly, NOS2 is upregulated in osteoarthritis and contributes to catabolism of cartilage via production of excess NO [31]. However, NOS3 has been shown to exert protective effects on cartilage integrity and homeostasis [32]. The excess NO generated by NOS2 can directly stimulate the production of pro-inflammatory cytokines such as IL-1β and TNF-α, which further perpetuate the inflammatory response and contribute to degradation of cartilage matrix [33]. The articular cartilage, which lacks vascular tissue, is commonly exposed to a hypoxic environment where the partial oxygen pressure decreases from 6 % at the surface to 1 % in the deep layers. Within articular cartilage cells, there is expression of HIF-1α, a primary regulatory factor involved in the hypoxic response. The HIF-1α pathway plays a crucial role in bone development and remodeling, particularly in regulating chondrocyte growth and differentiation [19]. A lack of HIF-1α protein expression in articular cartilage leads to marked chondrocyte death. Expression of HIF-1α is upregulated in a hypoxic environment, leading to the activation of downstream genes such as IL-1β, TNF-α, VEGF and NOS2, further exacerbating osteoarthritis pathology [34]. Importantly, NO was reported not only to modulate the HIF-1 response under hypoxic conditions, but to also function as an inducer of HIF-1. Accumulation of HIF-1 was reported to occur in both hypoxia as well as inflammatory conditions characterized by sustained NO production [35]. While HIF itself lacks the ability to detect changes in oxygen partial pressure, the prolylhydroxylase domain (PHD) plays a crucial role in sensing and regulating relevant changes to maintain stable levels of HIF-1α and ensure physiological function. As the rate-limiting enzyme for HIF1-α proline hydroxylation, PHD serves as one of the key regulatory factors responsible for HIF1-α degradation [36]. Arginine is a precursor to NO, which is synthesized from L-arginine by a variety of NOS isoforms [37].

Our in vivo experiments revealed that MJD effectively downregulates HIF1-α and NOS2 expression in the knee cartilage of KOA group rats. Furthermore, significant differences were observed in serum *cis*-4-hydroxy-D-proline and L-arginine levels among MJD and KOA group rats, as revealed by serum metabolomics analysis. Additionally, the molecular docking results indicated that the active constituents present in MJD exhibited potential interactions with relevant target proteins (i.e. ATK1, HF1A, VEGFA, NOS2 and NOS3), thereby suggesting their pharmacological efficacy as bioactive compounds. However, the specific pharmacodynamic effects of these MJD components require further verification through in vivo and in vitro research. Here, we found that MJD influences the early inflammatory microenvironment and subchondral microcirculation of joints affected by KOA via the modulation of arginine and proline metabolism pathways, as well as HIF signaling pathway. These mechanisms, in turn, ultimately produced an analgesic effect and enhanced the preservation of cartilage integrity.

Despite our promising findings, this study was not without limitations. Our research primarily focused on early-stage KOA in rats, and future research on the efficacy of MJD throughout different stages of KOA and other pathologies is warranted, especially in humans. As MJD consists of several herbs, each of the various bioactive compounds may contribute to its therapeutic effects in KOA management. Further research is warranted to investigate individual compound activity and explore potential synergistic effects among these various compounds. Understanding such likely synergistic mechanisms, in turn, may lead to the development of more effective and targeted treatments for KOA and other diseases.

In this study, a comparative analysis was conducted to evaluate MJD components obtained via LC-Q-TOF-MS and network pharmacological analysis. Findings revealed that of the 228 constituents, six were identical, namely glycyrrhizic acid, kuwanon C, betulinic acid, umbelliferone, citric acid and gentiopicroside. Furthermore, glycyrrhizic acid, kuwanon C and betulinic acid ranked among the top 20 active ingredients based on their mass spectrum response values. Glycyrrhizic acid has the ability to suppress the inflammatory response of chondrocytes [38]. Kuwanon C influences arachidonate metabolism by inhibiting Cyclooxygenase (COX) 1 and COX-2. It also inhibits the production of NO and platelet-activating factor, as well as arachidonic acid-induced platelet aggregation [39]. Betulinic acid demonstrated a dose-dependent inhibition of IL-1β-induced MMP-1, MMP-3, MMP-13, PGE2 and NO production in a study of IL-1β-stimulated human osteoarthritic chondrocytes [40]. Among the other top 20 active ingredients ranked by mass spectrum response values, kirenol and fukanefurochromone A may exhibit therapeutic effects on osteoarthritis pathology. Kirenol exerts a protective effect in collagen-induced arthritis animal models by inhibiting the migration, proliferation and invasion of synovial fibroblasts, as well as suppressing the secretion of inflammatory cytokines by synovial fibroblasts [41]. Stimulation of cultured chondrocytes with IL-1β confirmed that pretreatment with kirenol significantly attenuates IL-1β-induced production of NO, PGE2, TNF-α, IL-6 and NOS2 expression [42]. Fukanefurochromone A exhibits inhibitory effects on the production of NO and expression of NOS2 [43]. This further demonstrates the potential effectiveness of MJD in the treatment of early KOA by exerting anti-inflammatory effects and improving microcirculatory function. Finally, our findings underscored the limitations of network pharmacology analysis in light of its reliance on a singular, computational methodology based on public databases, which restricted its predictive capacity for compound-target combinations and pathway analysis.

5. Conclusion

In this study, we utilized an innovative and integrated approach to elucidate pivotal targets and mechanisms of MJD in the treatment of early-stage KOA by employing metabolomics and network pharmacology analyses. Our findings revealed two crucial targets along with relevant metabolites and pathways. These targets were further validated by molecular docking analysis and in vivo experimentation. Our research empirically and theoretically warrants further, in-depth clinical study of the underlying mechanisms of MJD to potentially develop novel, efficacious therapeutic agents. Finally, this study not only provides valuable insight into the intricate mechanisms of MJD in the treatment of KOA, but also emphasizes the advantages of employing a comprehensive approach to research TCM compounds.

Funding

This work was supported by grants from the program of the National Natural Science Foundation of China (82104884); Guangdong Basic and Applied Basic Research Foundation (2020A1515110559); and Traditional Chinese Medicine Bureau of Guangdong Province (20221356).

Data availability

The data that support the findings of this study are available from the corresponding author upon reasonable request.

Ethical approval

All animal protocols were approved (number: 2022-283) by the Animal Care and Use Committee of Shenzhen PKU-HKUST Medical Center. All experiments were conducted in accordance with the National Institutes of Health Guidelines for the Care and Use of Laboratory Animals.

CRediT authorship contribution statement

Kun Gao: Conceptualization. **Zhenyu Huang:** Writing – review & editing, Writing – original draft, Methodology. **Weiji Yu:** Methodology. **Yihong Wu:** Methodology. **Weidong Liu:** Methodology. **Shufen Sun:** Methodology. **Yong Zhang:** Methodology. **Dayu Chen:** Writing – review & editing, Methodology.

Declaration of competing interest

The authors declare that they have no known competing financial interests or personal relationships that could have appeared to influence the work reported in this paper.

Appendix A. Supplementary data

Supplementary data to this article can be found online at https://doi.org/10.1016/j.heliyon.2024.e30828.

References

[1] D.J. Hunter, S. Bierma-Zeinstra, Osteoarthritis, Lancet (London, England) 393 (2019) 1745–1759.
[2] P.K. Sacitharan, T.L. Vincent, Cellular ageing mechanisms in osteoarthritis, Mammalian genome, official journal of the International Mammalian Genome Society 27 (2016) 421–429.
[3] E.R. Vina, C.K. Kwoh, Epidemiology of osteoarthritis: literature update, Curr. Opin. Rheumatol. 30 (2018) 160–167.
[4] A. Mahmoudian, L.S. Lohmander, A. Mobasheri, M. Englund, F.P. Luyten, Early-stage symptomatic osteoarthritis of the knee - time for action, Nat. Rev. Rheumatol. 17 (2021) 621–632.
[5] W. Zhang, G. Nuki, R.W. Moskowitz, S. Abramson, R.D. Altman, N.K. Arden, S. Bierma-Zeinstra, K.D. Brandt, P. Croft, M. Doherty, M. Dougados, M. Hochberg, D.J. Hunter, K. Kwoh, L.S. Lohmander, P. Tugwell, OARSI recommendations for the management of hip and knee osteoarthritis: part III: changes in evidence following systematic cumulative update of research published through January 2009, Osteoarthritis Cartilage 18 (2010) 476–499.
[6] A. Fratianni, R. Ribeiro Da Costa, E.L. Leung Ki, M. Drepper, [Prevention of high digestive hemorrhage on NSAID], Rev. Med. Suisse 16 (2020) 268–271.
[7] X. Wang, A. Zhang, H. Sun, Future perspectives of Chinese medical formulae: chinmedomics as an effector, OMICS A J. Integr. Biol. 16 (2012) 414–421.
[8] Q. Wang, Y.R. Wang, Q.Y. Jia, L. Liu, C.Q. Xu, X.Y. Wang, M. Yao, L.S. Cui, Q. Shi, Y.J. Wang, Q.Q. Liang, The efficacy of the traditional Chinese medicine Juanbi pill combined with methotrexate in active rheumatoid arthritis: study protocol for a randomized controlled trial, Trials 19 (2018) 188.
[9] T. Wang, Q. Jia, T. Chen, H. Yin, X. Tian, X. Lin, Y. Liu, Y. Zhao, Y. Wang, Q. Shi, C. Huang, H. Xu, Q. Liang, Alleviation of synovial inflammation of juanbi-tang on collagen-induced arthritis and TNF-tg mice model, Front. Pharmacol. 11 (2020) 45.
[10] H. Zhou, L. Huang, K. Zhan, X. Liu, Wenhua Juanbi recipe attenuates rheumatoid arthritis via inhibiting miRNA-146a-mediated autophagy, BioMed Res. Int. 2022 (2022) 1768052.
[11] J. Gertsch, Botanical drugs, synergy, and network pharmacology: forth and back to intelligent mixtures, Planta Med. 77 (2011) 1086–1098.
[12] Y. Zhong, J. Luo, T. Tang, P. Li, T. Liu, H. Cui, Y. Wang, Z. Huang, Exploring pharmacological mechanisms of xuefu zhuyu decoction in the treatment of traumatic brain injury via a network pharmacology approach, evidence-based complementary and alternative medicine, eCAM 2018 (2018) 8916938.
[13] C. Fu, Q. Wu, Z. Zhang, Z. Xia, H. Ji, H. Lu, Y. Wang, UPLC-ESI-IT-TOF-MS metabolomic study of the therapeutic effect of Xuefu Zhuyu decoction on rats with traumatic brain injury, J. Ethnopharmacol. 245 (2019) 112149.
[14] S.R. Chaplan, F.W. Bach, J.W. Pogrel, J.M. Chung, T.L. Yaksh, Quantitative assessment of tactile allodynia in the rat paw, J. Neurosci. Methods 53 (1994) 55–63.
[15] S.K. Bulstra, W.A. Buurman, G.H. Walenkamp, A.J. Van der Linden, Metabolic characteristics of in vitro cultured human chondrocytes in relation to the histopathologic grade of osteoarthritis, Clin. Orthop. Relat. Res. (1989) 294–302.
[16] M.K. Skjødt, Y. Ostadahmadli, B. Abrahamsen, Long term time trends in use of medications associated with risk of developing osteoporosis: nationwide data for Denmark from 1999 to 2016, Bone 120 (2019) 94–100.
[17] R. van Lutterveld, K.M. Diederen, W.M. Otte, I.E. Sommer, Network analysis of auditory hallucinations in nonpsychotic individuals, Hum. Brain Mapp. 35 (2014) 1436–1445.
[18] J. Xie, J. Lin, M. Wei, Y. Teng, Q. He, G. Yang, X. Yang, Sustained Akt signaling in articular chondrocytes causes osteoarthritis via oxidative stress-induced senescence in mice, Bone research 7 (2019) 23.
[19] H. Zhang, L. Wang, J. Cui, S. Wang, Y. Han, H. Shao, C. Wang, Y. Hu, X. Li, Q. Zhou, J. Guo, X. Zhuang, S. Sheng, T. Zhang, D. Zhou, J. Chen, F. Wang, Q. Gao, Y. Jing, X. Chen, J. Su, Maintaining hypoxia environment of subchondral bone alleviates osteoarthritis progression, Sci. Adv. 9 (2023) eabo7868.

[20] S. Takano, K. Uchida, G. Inoue, T. Matsumoto, J. Aikawa, D. Iwase, M. Mukai, M. Miyagi, M. Takaso, Vascular endothelial growth factor expression and their action in the synovial membranes of patients with painful knee osteoarthritis, BMC Muscoskel. Disord. 19 (2018) 204.

[21] P. Teng, Y. Liu, Y. Dai, H. Zhang, W.T. Liu, J. Hu, Nicotine attenuates osteoarthritis pain and matrix metalloproteinase-9 expression via the α7 nicotinic acetylcholine receptor, Journal of immunology (Baltimore, Md. : 1950 203 (2019) 485–492.

[22] J. Xiao, P. Zhang, F.L. Cai, C.G. Luo, T. Pu, X.L. Pan, M. Tian, IL-17 in osteoarthritis: a narrative review, Open Life Sci. 18 (2023) 20220747.

[23] O. Stannus, G. Jones, F. Cicuttini, V. Parameswaran, S. Quinn, J. Burgess, C. Ding, Circulating levels of IL-6 and TNF-α are associated with knee radiographic osteoarthritis and knee cartilage loss in older adults, Osteoarthritis Cartilage 18 (2010) 1441–1447.

[24] A. Nair, V. Kanda, C. Bush-Joseph, N. Verma, S. Chubinskaya, K. Mikecz, T.T. Glant, A.M. Malfait, M.K. Crow, G.T. Spear, A. Finnegan, C.R. Scanzello, Synovial fluid from patients with early osteoarthritis modulates fibroblast-like synoviocyte responses to toll-like receptor 4 and toll-like receptor 2 ligands via soluble CD14, Arthritis Rheum. 64 (2012) 2268–2277.

[25] P. Lepetsos, A.G. Papavassiliou, ROS/oxidative stress signaling in osteoarthritis, Biochim. Biophys. Acta 1862 (2016) 576–591.

[26] S. Cao, Y. Li, R. Song, X. Meng, M. Fuchs, C. Liang, K. Kachler, X. Meng, J. Wen, U. Schlötzer-Schrehardt, V. Taudte, A. Gessner, M. Kunz, U. Schleicher, M. M. Zaiss, A. Kastbom, X. Chen, G. Schett, A. Bozec, L-arginine metabolism inhibits arthritis and inflammatory bone loss, Annals of the rheumatic diseases 83 (2024) 72–87.

[27] R. Chen, S. Han, X. Liu, K. Wang, Y. Zhou, C. Yang, X. Zhang, Perturbations in amino acids and metabolic pathways in osteoarthritis patients determined by targeted metabolomics analysis, J. Chromatogr., B: Anal. Technol. Biomed. Life Sci. 1085 (2018) 54–62.

[28] M. Binvignat, P. Emond, F. Mifsud, B. Miao, A. Courties, A. Lefèvre, E. Maheu, M.D. Crema, D. Klatzmann, M. Kloppenburg, P. Richette, A.J. Butte, E. Mariotti-Ferrandiz, F. Berenbaum, H. Sokol, J. Sellam, Serum tryptophan metabolites are associated with erosive hand osteoarthritis and pain: results from the DIGICOD cohort, Osteoarthritis Cartilage 31 (2023) 1132–1143.

[29] Z. Huang, Z. He, Y. Kong, Z. Liu, L. Gong, Insight into osteoarthritis through integrative analysis of metabolomics and transcriptomics, Clinica chimica acta; international journal of clinical chemistry 510 (2020) 323–329.

[30] S.B. Abramson, Osteoarthritis and nitric oxide, Osteoarthritis Cartilage 16 (Suppl 2) (2008) S15–S20.

[31] R.F. Loeser, C.S. Carlson, M. Del Carlo, A. Cole, Detection of nitrotyrosine in aging and osteoarthritic cartilage: correlation of oxidative damage with the presence of interleukin-1beta and with chondrocyte resistance to insulin-like growth factor 1, Arthritis Rheum. 46 (2002) 2349–2357.

[32] J.P. Pelletier, V. Lascau-Coman, D. Jovanovic, J.C. Fernandes, P. Manning, J.R. Connor, M.G. Currie, J. Martel-Pelletier, Selective inhibition of inducible nitric oxide synthase in experimental osteoarthritis is associated with reduction in tissue levels of catabolic factors, J. Rheumatol. 26 (1999) 2002–2014.

[33] B. Fermor, J.B. Weinberg, D.S. Pisetsky, M.A. Misukonis, A.J. Banes, F. Guilak, The effects of static and intermittent compression on nitric oxide production in articular cartilage explants, J. Orthop. Res. : official publication of the Orthopaedic Research Society 19 (2001) 729–737.

[34] V. Wang, D.A. Davis, M. Haque, L.E. Huang, R. Yarchoan, Differential gene up-regulation by hypoxia-inducible factor-1alpha and hypoxia-inducible factor-2alpha in HEK293T cells, Cancer Res. 65 (2005) 3299–3306.

[35] K.B. Sandau, J. Fandrey, B. Brüne, Accumulation of HIF-1alpha under the influence of nitric oxide, Blood 97 (2001) 1009–1015.

[36] D. You, D. Du, X. Zhao, X. Li, M. Ying, X. Hu, Mitochondrial malic enzyme 2 promotes breast cancer metastasis via stabilizing HIF-1α under hypoxia, Chinese journal of cancer research = Chung-kuo yen cheng yen chiu 33 (2021) 308–322.

[37] H.Y. He, A.C. Henderson, Y.L. Du, K.S. Ryan, Two-enzyme pathway links l-arginine to nitric oxide in N-nitroso biosynthesis, J. Am. Chem. Soc. 141 (2019) 4026–4033.

[38] C. Li, L. Li, T. Lan, Co-treatment with disulfiram and glycyrrhizic acid suppresses the inflammatory response of chondrocytes, J. Orthop. Surg. Res. 16 (2021) 132.

[39] H. Zelová, Z. Hanáková, Z. Čermáková, K. Šmejkal, S. Dall´Acqua, P. Babula, J. Cvačka, J. Hošek, Evaluation of anti-inflammatory activity of prenylated substances isolated from Morus alba and Morus nigra, Journal of natural products 77 (2014) 1297–1303.

[40] W. Jingbo, C. Aimin, W. Qi, L. Xin, L. Huaining, Betulinic acid inhibits IL-1β-induced inflammation by activating PPAR-γ in human osteoarthritis chondrocytes, Int. Immunopharm. 29 (2015) 687–692.

[41] J. Wu, Q. Li, L. Jin, Y. Qu, B.B. Liang, X.T. Zhu, H.Y. Du, L.G. Jie, Q.H. Yu, Kirenol inhibits the function and inflammation of fibroblast-like synoviocytes in rheumatoid arthritis in vitro and in vivo, Front. Immunol. 10 (2019) 1304.

[42] W. Hu, C. Mao, W. Sheng, The protective effect of kirenol in osteoarthritis: an in vitro and in vivo study, J. Orthop. Surg. Res. 17 (2022) 195.

[43] Z. Ghasemi, R. Rezaee, M.R. Aslani, M.H. Boskabady, Anti-inflammatory, anti-oxidant, and immunomodulatory activities of the genus Ferula and their constituents: a review, Iranian journal of basic medical sciences 24 (2021) 1613–1623.